Acta Oceanol. Sin., 2017, Vol. 36, No. 6, P. 23–33
DOI: 10.1007/s13131-016-0965-z
http://www.hyxb.org.cn
E-mail: hyxbe@263.net

Vertical development of a *Prorocentrum donghaiense* bloom in the coastal waters of the East China Sea: coupled biophysical numerical modeling

SUN Ke[1, 2], QIU Zhongfeng[3]*, HE Yijun[3], FAN Wei[4], WEI Zexun[1, 2]

[1] The First Institute of Oceanography, State Oceanic Administration, Qingdao 266061, China

[2] Laboratory for Regional Oceanography and Numerical Modeling, Qingdao National Laboratory for Marine Science and Technology, Qingdao 266071, China

[3] School of Marine Sciences, Nanjing University of Information Science and Technology, Nanjing 210044, China

[4] Ocean College, Zhejiang University, Hangzhou 310058, China

Received 23 December 2015; accepted 17 February 2016

Abstract

Algal blooms caused by *Prorocentrum donghaiense* occurred frequently in the East China Sea (ECS) during spring in recent years. In this study, a coupled biophysical model was used to hindcast a massive *P. donghaiense* bloom that occurred in 2005 and to determine the factors influencing bloom initiation and development. The model comprised the Regional Ocean Modeling System tailored for the ECS that utilized a multi-nested configuration and a population dynamics model for *P. donghaiense*. Comparisons between simulations and observations revealed that the biological model is capable of reproducing the characteristics of *P. donghaiense* growth under different irradiances and phosphorus limitation scenarios. The variation of intracellular phosphorus and the effects of *P. donghaiense* on ambient nutrients conditions were also reproduced. The biophysical model hindcasted the hydrodynamics and spatiotemporal distributions of the *P. donghaiense* bloom reasonably well. Bloom development was consistent with observations reported in earlier studies. The results demonstrate the capability of the model in capturing subsurface incubation during bloom initiation. Then model's hindcast solutions were further used to diagnose the factors controlling the vertical distribution. Phosphate appeared to be one of the factors controlling the subsurface incubation, whereas surface wind fields played an important role in determining *P. donghaiense* distribution. The results highlight the importance of nutrient-limitation as a mechanism in the formation of *P. donghaiense* subsurface layers and the dispersing of *P. donghaiense* blooms. This coupled biophysical model should be improved and used to investigate *P. donghaiense* blooms occurring in different scenarios.

Key words: *Prorocentrum donghaiense*, algal blooms, biophysical model, subsurface incubation, East China Sea

Citation: Sun Ke, Qiu Zhongfeng, He Yijun, Fan Wei, Wei Zexun. 2017. Vertical development of a *Prorocentrum donghaiense* bloom in the coastal waters of the East China Sea: coupled biophysical numerical modeling. Acta Oceanologica Sinica, 36(6): 23–33, doi: 10.1007/s13131-016-0965-z

1 Introduction

In recent years, large-scale harmful algal blooms occurred frequently in coastal areas of China. In particular, blooms of the dinoflagellate *Prorocentrum donghaiense* (affected 1 000–10 000 km^2 for more than 30 d) have been a recurrent phenomenon in spring in the East China Sea (ECS) since the 1990s (Zhou et al., 2003, 2006). Previous investigations indicate that *P. donghaiense* blooms may be regulated by a suite of complex biological and physical processes (Chen et al., 2006; Tang et al., 2006; Sun et al., 2008; Zhu et al., 2009; Li et al., 2011). Characterizing environmental variability and understanding how physical and biological factors govern bloom initiation and development have therefore been the focus of *P. donghaiense* bloom dynamic studies.

In addition, the fine-scale vertical distributions of phytoplankton are considered important hotspots of ecological activity; for example, the thin layer found in the coastal ocean, meters beneath the surface, contains phytoplankton up to two orders of magnitude above ambient concentrations (Durham et al., 2009). A large number of harmful algal species have been observed in these thin layers (McManus et al., 2008; Rines et al., 2002, 2010; Sullivan et al., 2003, 2005, 2010) highlighting the importance of understanding the vertical distribution in harmful algal blooms research. *Prorocentrum donghaiense* requires retention zones or other small-scale structures for populations development; these zones are thought to be incubators for subsequent massive *P. donghaiense* blooms (Zhou and Zhu, 2006). For example, *P. donghaiense* remained at the subsurface/middle layer for one month in early April 2004, this lead to the later development of massive bloom (Zhou and Zhu, 2006). In 2005, *Karenia mikimotoi* became the dominant species followed by *P. donghaiense* in the subsurface/middle layer, leading to the outbreak of a large bloom in late May (Zhou and Zhu, 2006).

Several mechanisms have been proposed to explain the formation and persistence of thin layers (Durham and Stocker, 2012);

Foundation item: The National Natural Science Foundation of China (NSFC) under contract Nos 41276186, 41506015 and 41606038; the NSFC—Shandong Joint Fund for Marine Science Research Centers under contract No. U1606405; the Postdoctoral Innovation Foundation of Shandong Province under contract No. 201502031.
*Corresponding author, E-mail: zhongfeng.qiu@nuist.edu.cn

current interpretations of their formation favor abiotic processes (Durham et al., 2009). However, the mechanisms responsible for the formation and persistence of *P. donghaiense* subsurface layers remain inconclusive and require further investigation. The 2005 bloom season provided an opportunity to determine the factors influencing the vertical distributions of *P. donghaiense* blooms, since intensive measurements and sampling were undertaken during this period (Zhang et al., 2008). *In-situ* observations and numerical models can form a complementary approach to such investigations. While *in-situ* observations provide valuable information for describing physical and biological conditions, they are spatially and temporally limited in the depiction of bloom evolution. In contrast, numerical models can reproduce continuous pictures of blooms, and reveal the underlying physical or biological mechanisms. The purpose of this paper was to utilize a coupled biophysical model to hindcast a massive *P. donghaiense* bloom that occurred in 2005, with particular focus on its vertical development.

2 Data and methods

The coupled modeling system comprised a circulation model and a biological model describing the growth of diatoms (represented by *Skeletonema costatum*) and dinoflagellates (represented by *P. donghaiense*). Note that the interaction such as allelopathy between diatoms and dinoflagellates is not considered in the model. The physical model provided the fields of velocity, turbulence diffusivity, temperature, and salinity to the biological model.

2.1 *Biological model*

The *S. costatum*-specific model has been described in Sun et al. (2014). One of our main objectives in the present study was to develop, as much as possible, a *P. donghaiense*-specific model based on theoretical formulas and laboratory-yielded parameters. The biological model was a multi-component model involving *P. donghaiense* and two dissolved inorganic nutrients (nitrate [NO_3^-] and phosphate [PO_4^{3-}]). The growth rate of *P. donghaiense* is influenced by the temperature, salinity, irradiance, and nutrients. Interested readers are referred to Sun et al. (2014) for a detailed description of the *S. costatum*-specific model with a similar structure. Here, the changes made to the original model structure (Sun et al., 2014) are emphasized.

In contrast with the *S. costatum* model, the *P. donghaiense* model does not include silicon-related components. In addition, the effect of temperature and salinity on *P. donghaiense* growth is depicted as per Xu et al. (2010) (Eq. (1)). Previous investigations show that *P. donghaiense* can grow only in the temperature and salinity ranges of 10–31°C and 15–40, respectively (You, 2006; Zhao, 2006; Deng et al., 2009). Therefore, the temperature (T) and salinity (S) limitation relative to the maximum growth are shown as

$$\begin{cases} f_{TS} = (-1.982\,46 + 0.121\,461T + 0.085\,4S - \\ \qquad 0.005\,13TS - 0.000\,12T^3 + 0.000\,226T^2S - \\ \qquad 0.000\,057TS^2 - 0.000\,004\,7S^3)/0.867, \\ \qquad (R^2 = 0.906)\ 10^\circ\mathrm{C} \leqslant T < 31^\circ\mathrm{C} \text{ and } 15 \leqslant S < 40, \\ f_{TS} = 0 \text{ if } T < 10^\circ\mathrm{C} \text{ or } T > 31^\circ \text{ and } S < 15^\circ \text{ or } S > 40. \end{cases} \quad (1)$$

Before coupling with the circulation model, the biological model was calibrated and validated against the results of published laboratory experiments. All strains used in these experiments were isolated from the ECS. The set conditions of numerical tests were the same as that used in each experiment, including initial cell concentrations, nutrient concentrations (NO_3^- and PO_4^{3-}), temperature, salinity, and irradiance. The carbon (C) content of *P. donghaiense* cells was set as a constant 207 pg/cell (Chen et al., 2007) and the initial chlorophyll *a* (Chl *a*) content was set as 1 pg/cell (Lu, 2005; Sun and Duan, 2006; Zhao, 2006; Zhao et al., 2009). We set the initial content ratios of nitrogen (N)/C and phosphorus (P)/C as an average (i.e., equal to the mean of the minimum and maximum values) unless noted otherwise. The culture media were assumed homogeneous in the model since they were stirred daily in the experiments. A scattergram was used to assess the calibration and validation in accordance with Sun et al. (2014).

2.1.1 *Calibration*

We tested the sensitivity of state variables (cell concentration, Chl *a*, NO_3^-, and PO_4^{3-}) to different parameters under N- or P-limiting conditions (results not shown). The photosynthetic and quota parameters are always the most influential, although results vary depending on the state variables and culture conditions. These parameters were then calibrated via an ad hoc method (manual adjustment of parameter values) and a model parameter estimation modeling software (Doherty, 2004). The ranges of most parameter values were derived from *P. donghaiense* experiments reported in the literature.

We used the experimental results of Xu et al. (2010) to calibrate photosynthetic parameters. In the experiment, eleven irradiance levels (2, 4, 7, 15, 30, 60, 90, 110, 140, 170, and 230 μmol quanta m^{-2} s^{-1}) were used in a 12 h : 12 h light:dark cycle. Cell concentrations were assessed daily, and the specific growth rates (d^{-1}) in the exponential growth phase were calculated according to Guillard (1973). The experimental results by Lai et al. (2011) were used to calibrate the quota parameters. In the experiment, four PO_4^{3-} levels (0, 2, 4, and 8 μmol/L) were used in each treatment where NO_3^- was sufficient. The irradiance level was 45 μmol quanta m^{-2} s^{-1} in a 12 h : 12 h light:dark cycle.

2.1.2 *Validation*

We used two experiments to validate model parameters and test the model's ability to represent *P. donghaiense* growth. The first experiment was performed by You (2006) to investigate the effect of irradiance *P. donghaiense* growth. In the experiment, four different irradiance levels (10, 30, 55, and 100 μmol quanta m^{-2} s^{-1}) were used in a 12 h : 12 h light:dark cycle. The other experiment comprised a P uptake assessment as performed by Huang et al. (2005) to test the bioavailability of PO_4^{3-} to *P. donghaiense*. In their experiment, the initial concentrations of cells, NO_3^-, and PO_4^{3-} were 1×10^4 cells/mL, 882 μmol/L, and 5.4 μmol/L, respectively. The irradiance level was 88 μmol quanta m^{-2} s^{-1} in a 14 h : 10 h light:dark cycle. The set concentration of cell and nutrients were the same as those reported by Huang et al. (2005). In addition, the initial cellular P quota was set at 0.072 9 pmol/cell according to the experimental results.

2.2 *Circulation model*

The circulation model was based on the Regional Ocean Modeling System (ROMS http://www.myroms.org/), a free-surface, hydrostatic and primitive-equation model based on the nonlinear terrain-following coordinate (Song and Haidvogel, 1994). Details of the ROMS computational algorithms have been reported by Shchepetkin and McWilliams (2005). The central model domain (Fig. 1) extended from 27°N to 33°N and from 119°30′E to 125°E with a horizontal resolution of 2 km and 24 levels in the vertical. To overcome the difficulties associated with defining open boundary conditions for the regional coastal circulation model, we implemented a multi-nested configuration. Given the nature of one-way nesting, the climatology simulations of Nest 1, Nest 2, and Nest 3 were performed in sequential order, in which only the hydrodynamics were computed. Following this,

the Nest 3 hindcast from January 1 to June 30 in 2005 was carried out, in which both the hydrodynamics and algal populations were simultaneously simulated. Interested readers are referred to Sun et al. (2016) for more details on the circulation model.

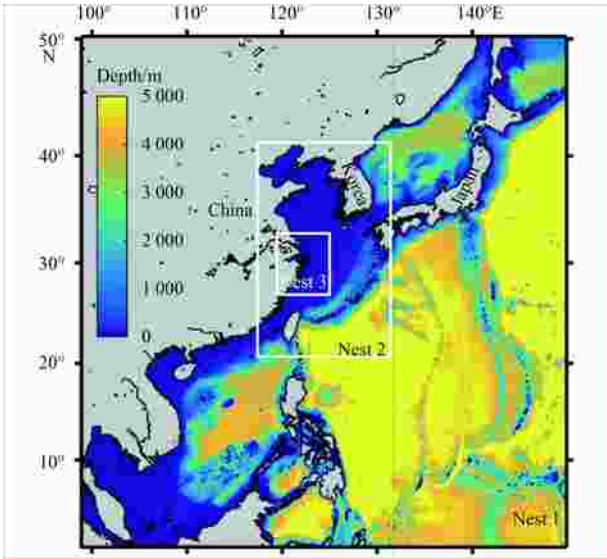

Fig. 1. Domains of the one-way nested model Nest 1, Nest 2, and Nest 3.

3 Results

3.1 *Calibration results*

The model was fit to the experimental data, and the obtained parameter values (Table 1) are in the ranges reported by the literature. In order to buffer the large fluctuations caused by the photosynthesis parameters, we used parameter B and set it to 10 in order to match the growth dynamics of observations. Mortality was set to 0.35×10^{-6} s^{-1} in all of the experiments included in the calibration and validation; this value is within the range reported by Baklouti et al. (2006). Table 2 lists the other parameters used in the model.

Figures 2 and 3 show the comparisons between the simulated and observed data. The corresponding scattergrams are also presented. These figures show that the model outputs fit the experimental results well (R^2 between 0.72–0.99). We then used the adjusted parameters in the validation unless stated otherwise.

3.2 *Validation results*

The simulated results show that the growth rate and maximum biomass under 10 μmol quanta m^{-2} s^{-1} were significantly lower than those under the other three irradiances, as shown in Fig. 4. With elevations in irradiance, the growth rate increased rapidly until saturation at 30 μmol quanta m^{-2} s^{-1}. Similar to the model outputs, the experimental growth increased with irradiance and was saturated at low irradiance (~30 μmol quanta m^{-2} s^{-1}). This indicates that the model could approximately depict the effect of irradiance on *P. donghaiense* growth.

Variations in cell concentration, intracellular P, and PO_4^{3-} are shown in Fig. 5. The experimental results show that *P. donghaiense* grew exponentially with abundant supplementation of ambient PO_4^{3-} in the first two days (Fig. 5a), whereas the concentration of PO_4^{3-} decreased significantly and was maintained at zero (Fig. 5b). Figure 5c shows that excess P was stored in the intracellular P pool. Intracellular P was concentrated as high as 0.3 pmol/cell in the first day and then decreased gradually. When the PO_4^{3-} supply was exhausted, *P. donghaiense* could maintain its growth for several days as shown in Fig. 5a. During this period, *P. donghaiense* utilized its intracellular P to support growth, and the cell concentration reached a peak of 7×10^4 cells/mL. Growth halted when intracellular P decreased to 0.07 pmol/cell (Fig. 5c).

Table 1. Tuned parameter values in the model

Parameter	Symbol	Unit	Value
Mean Chl *a* specific absorption coefficient at 400–700 nm	$\overline{a}$	m^2/g	29
Maximum quantum yield of carbon fixation	ϕ_m^C	(mol C)/(mol quanta)	0.080 6
Effective cross-section of photosystem (PS) II	σ	m^2/quanta	550×10^{-20}
Turnover time of electron transfer	τ	s	1×10^{-2}
Minimum content ratio of nitrogen to carbon	$Q_{\min N}$	(mol N)/(mol C)	0.020 3
Maximum content ratio of nitrogen to carbon	$Q_{\max N}$	(mol N)/(mol C)	0.084 9
Minimum content ratio of phosphorus to carbon	$Q_{\min P}$	(mol P)/(mol C)	0.002 7
Maximum content ratio of phosphorus to carbon	$Q_{\max P}$	(mol P)/(mol C)	0.018 6
Maximum content ratio of Chl *a* to nitrogen	θ_m^N	(g Chl *a*)/(mol N)	2.64
Mortality	m	s^{-1}	0.35×10^{-6}
Buffer coefficient	B	–	10

Table 2. Other parameter values used in the model

Parameter	Symbol	Unit	Value	Reference
Dimensionless PS II damage rate	k_d^H	–	4.5×10^{-8}	Baklouti et al. (2006)
Repair rate of damaged PS II	k_r	s^{-1}	2.6×10^{-4}	Baklouti et al. (2006)
Half-saturation constant for NO_3^- uptake	k_{NO_3}	(mol N)/m^3	10.8×10^{-3}	Sun (2010), Xu (2006)
Half-saturation constant for PO_4^{3-} uptake	k_{PO}	(mol P)/m^3	1.5×10^{-3}	Deng (2004), Li (2006), Xu (2006), Ou et al. (2008)
Half-saturation inhibition constant	K_I	(mol N)/m^3	0.54×10^{-3}	Baklouti et al. (2006)
Maximum realized inhibition	I_m	–	0.72	Baklouti et al. (2006)
Respiration cost for growth	R_g	(mol C)/(mol C)	0.25	Baklouti et al. (2006)
Respiration cost for NO_3^- uptake	R_{u,NO_3}	(mol C)/(mol N)	0.4	Baklouti et al. (2006)
Respiration cost for NO_3^- reduction	R_{r,NO_3}	(mol C)/(mol N)	2	Baklouti et al. (2006)
Respiration cost for PO_4^{3-} uptake	R_{u,PO_4}	(mol C)/(mol P)	0.2	Cannell and Thornley (2000)

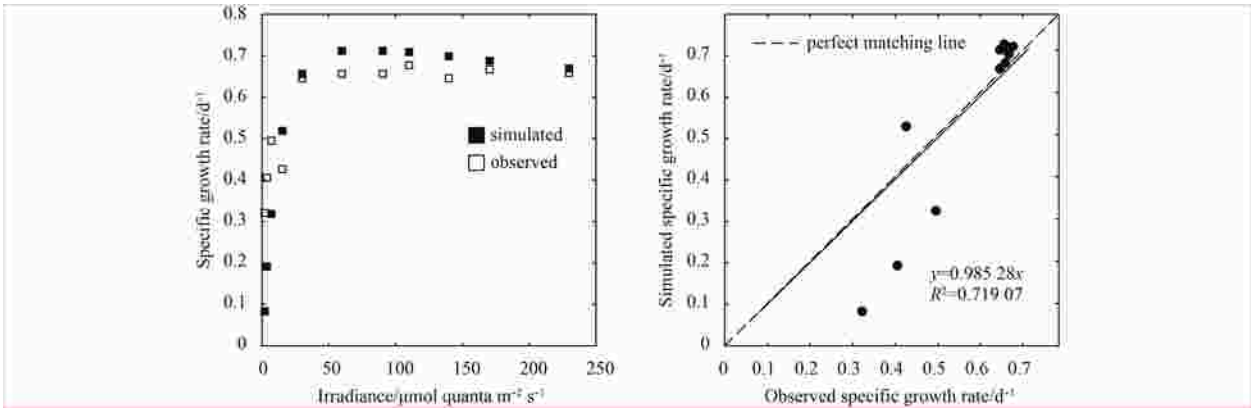

Fig. 2. Growth rate versus irradiance for *P. donghaiense* (data from Xu et al., 2010) and corresponding scattergram.

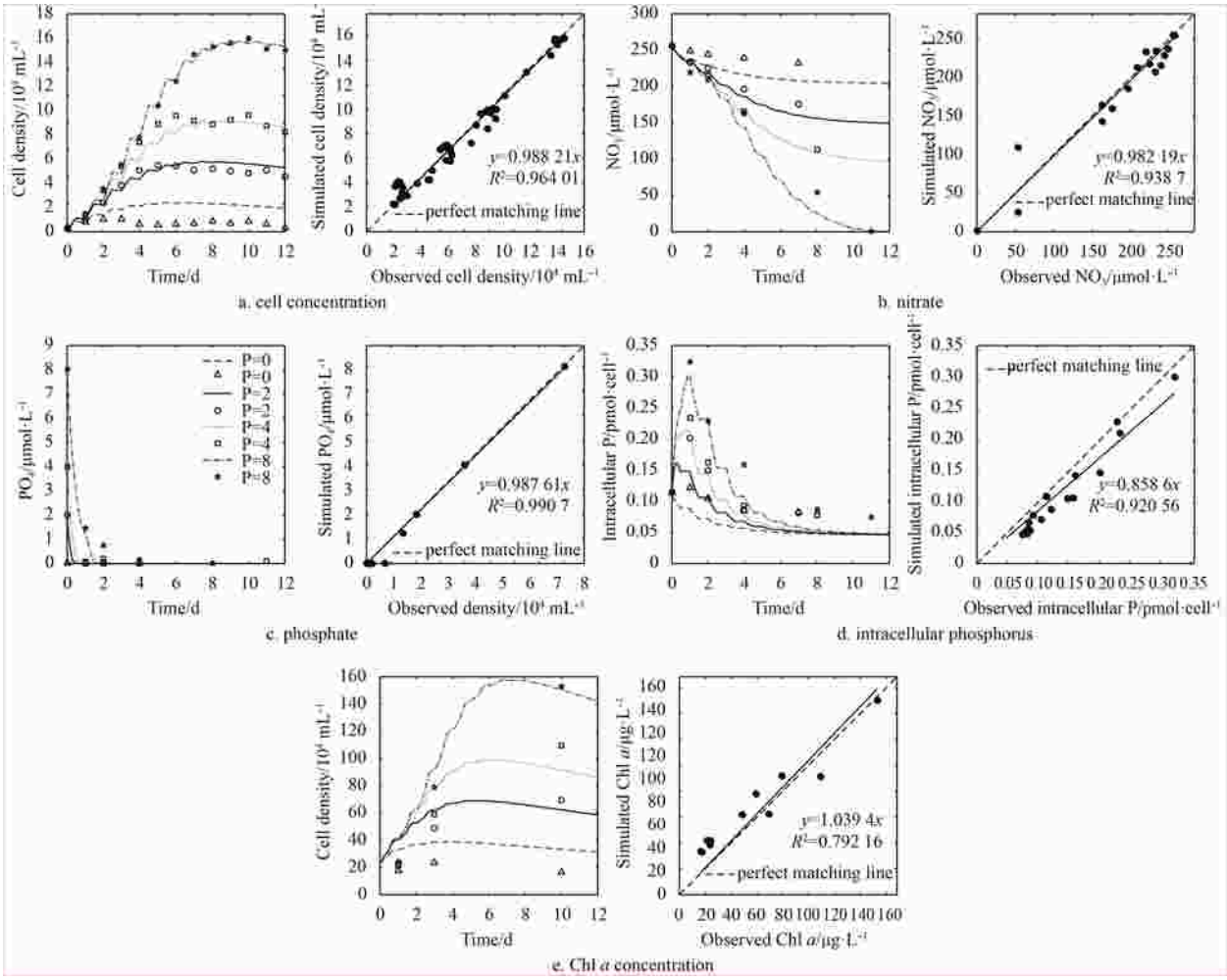

Fig. 3. Comparisons between the simulations (lines) and observations (data points) (data from Lai et al., 2011), and corresponding scattergrams. a. Cell concentration, b. nitrate, c. phosphate, d. intracellular phosphorus, and e. Chl *a* concentration.

The simulated results are in a good agreement with laboratory results of cell concentration, PO_4^{3-}, and intracellular P, indicating that the model can represent the growth dynamics of *P. donghaiense* and stoichiometry variations under P-limited conditions.

3.3 *Coupled model results*

Numerical models are advantageous for producing time- and space-continuous state variables from which important ocean physical and biological processes can be deduced. Extensive model-data comparisons are required, and hydrographic comparisons including temperature, salinity, and current have been described in the companion paper (Sun et al., 2016). In summary, these comparisons suggest that, in general, the model is capable of reproducing the observed hydrodynamics, increasing the confidence that the biological model is couched in a realistic physical environment. As discussed in the companion paper

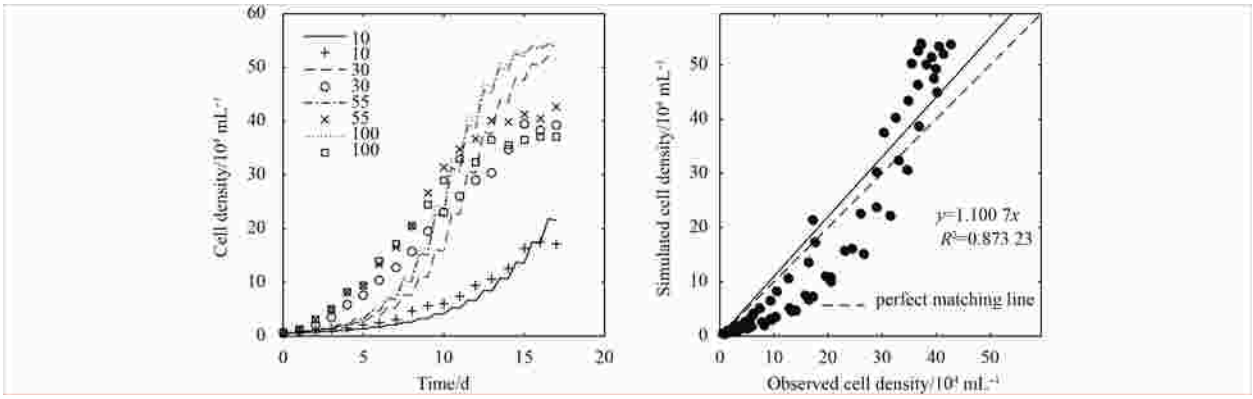

Fig. 4. Simulation of *P. donghaiense* growth under four irradiance levels and corresponding scattergram. Lines represent simulations and data points observations (data from You, 2006).

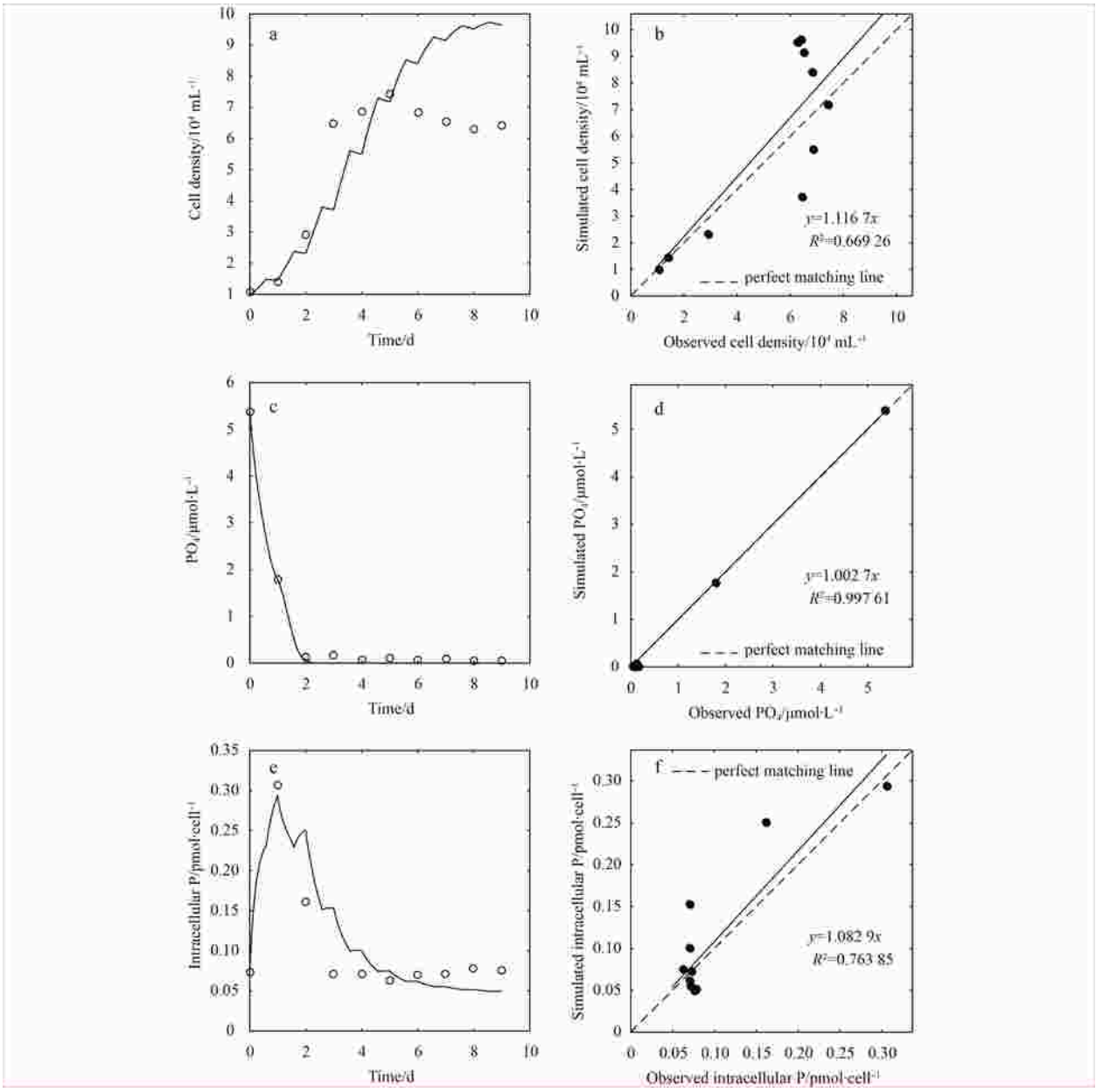

Fig. 5. Comparisons between the simulations (lines) and observations (data points) (data from Huang et al., 2005). a and b. Cell concentration, c and d. phosphate, and e and f. intracellular phosphorous.

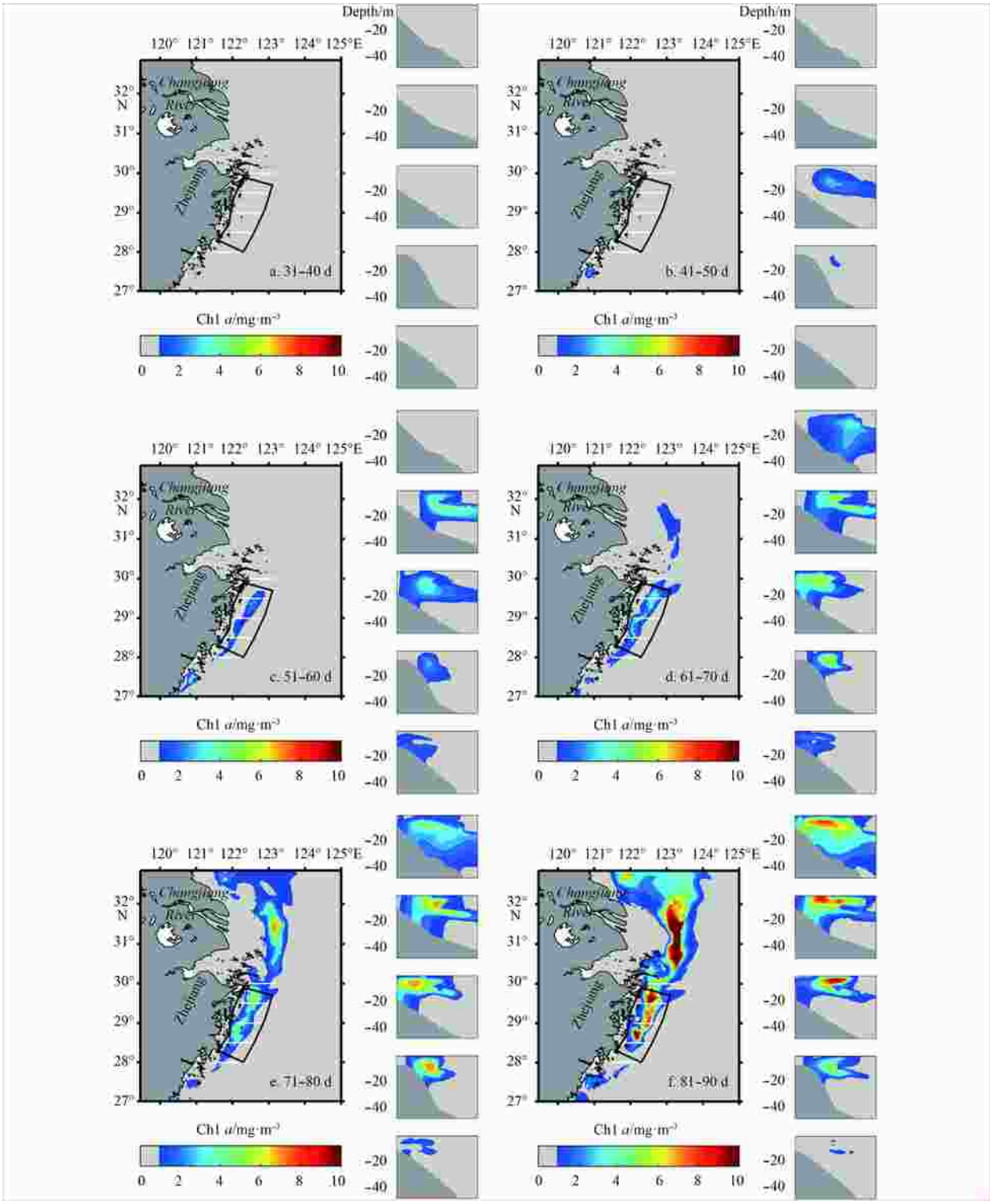

Fig. 6. Ten day-mean distributions of the three-dimensional *P. donghaiense* bloom. In each panel, the surface Chl *a* concentration map is displayed above five sections near the survey area showing both surface and vertical Chl *a* distributions. Maximum Chl *a* concentration is set to 10 mg/m^3 to highlight the threshold of the bloom. The survey region is marked by the black outline, corresponding to Fig. 1 shown in Sun et al. (2016).

(Sun et al., 2016), the dinoflagellate bloom initiated after April; therefore, only the outputs of the last 60 d (May and June) were analyzed and discussed. In the realistic physical environment and the observed nutrients field, the model reproduced an outbreak of *P. donghaiense* bloom in late June, consistent with previous observations (Zhang, 2008). Model realizations provide detailed illustrations of bloom evolution and the three-dimensional structure. This paper focused on the vertical distribution of the bloom, while the horizontal distribution is presented in the companion paper (Sun et al., 2016).

Before the 40th day, the Chl *a* concentration in the whole survey area was below 1 mg/m^3 (Fig. 6a). During the 40–50th days, while the surface concentration of Chl *a* was below 2 mg/m^3, the vertical profiles revealed higher Chl *a* concentrations (>3 mg/m^3) near the isobaths at 10–20 m depth (subsurface layer) (Fig. 6b). The Chl *a* concentrations in subsurface layer then became denser and gradually moved upward (Figs 6c, d and e). Ultimately, Chl *a* was largely concentrated at the surface waters, leading to the outbreak of a bloom (Fig. 6f). The incubation of Chl *a* in the subsurface layers agrees with observations (Fig. A1). Since subsurface incubation is believed to be recurrent in this area (Zhou and Zhu, 2006) and the vertical Chl *a* profiles in 2005 have not been published, the data in 2004 are shown to illustrate this phenomenon (Fig. A1).

4 Discussion

4.1 *Growth controlled by irradiance and P limitation*

We should initially discuss the indicator of phytoplankton biomass. In our model, both C and Chl *a* were formulated and could both be selected as indicators of phytoplankton biomass (Cullen, 1982). Since most results of the laboratory experiments used in Section 2.1 were based on cell concentrations, C was selected to estimate the biomass of *P. donghaiense*. The relationship between C and Chl *a* was well demonstrated in Figs 3a and e. Chl *a* was selected as the indicator of *P. donghaiense* biomass during the bloom simulation because the observations of *P. donghaiense* bloom were based on Chl *a*. Furthermore, Chl *a* is a better indicator to represent the effect of irradiance on the vertical distribution of *P. donghaiense*.

Previous investigations have confirmed that light significantly influences the growth of harmful algal species, and promotes the formation of blooms, especially in turbid environments such as the coastal area of the ECS (Xu et al., 2010). The optimum irradiance for *P. donghaiense* growth exceeds 30 μmol quanta m^{-2} s^{-1} (Sun, 2010; Xu et al., 2010; Dai et al., 2011); this is in agreement with the simulated results of the present study. The optimal light intensity for *P. donghaiense* growth is lower than that of several other algae (*Alexandrium tamarense*, *Karenia mikimotoi* and *Skeletonema costatum*), suggesting that *P. donghaiense* may have a blooming advantage in turbid environments (Sun et al., 2008). The present findings show that PO_4^{3-} was quickly taken up and stored in intracellular P-pools in the early stage of the experiment (Figs 3c and d; 5b and c), confirming that *P. donghaiense* is a luxury P consumer (Huang et al., 2005; Lai et al., 2011). In the model, the relationship between the primary production rate and internal pool of limiting nutrient (after Droop, 1968) enabled the model to capture these details.

4.2 *Factors governing vertical distribution of blooms*

Given that the coupled model could produce a generally credible hindcast of the hydrodynamics and *P. donghaiense* bloom in 2005, it can be used as a tool to investigate bloom evolution. Term-by-term diagnostics of the model governing equation allow the detailed evaluation of the relative importance of each potential controlling factor. We extract the data from the third section, which is located at the middle of the five sections shown in Fig. 6. Chl *a* was shown to mimics the spatiotemporal evolution of the gross Chl *a* synthesis rate (Figs 7a and b). Since mortality did not play a major role, the difference between the net synthesis term (Fig. 7c) and the gross synthesis rate (Fig. 7b) was negligible. In this regard, the analysis of terms regulating the gross synthesis rate is particular valuable. The gross synthesis rate reflects variations in C (Fig. 7d) and μ(E, N, P) (Fig. 7e). Chl *a* synthesis is confined to upper water since the distribution of C is limited in deep water due to light attenuation. Why does Chl *a* accumulate at the subsurface layers? We note that at the surface layers, the limited region of Chl *a* synthesis is consistent with μ(E, N, P) (Fig. 7e). This region could be divided into two parts (as shown in Fig. 7e). Both parts were limited by light at the surface layers (Fig. 7f), while nutrient limitation (Fig. 7g) especially PO_4^{3-} limitation (Fig. 7h) was more pronounced in the eastern part. In contrast, NO_3^- limitation (Fig. 7i) did not play a major role.

4.3 *Factors affecting bloom evolution*

Zhou and Zhu (2006) divided a time series of dinoflagellate blooms in the ESC into four stages: initiating, developing, proliferating, and dispersing. They also proposed the movement of cells in each stage, as listed in Table 3. Our simulated results captured a similar process of bloom evolution. Although the model did not reproduce the motion from the bottom to the subsurface at the initiating stage, the motion of Chl *a* from the subsurface to the surface was well reproduced. In Section 4.2, we concluded that Chl *a* synthesis might be limited by the intensive light and partially by nutrient limitation at the surface layers. As a result, Chl *a* was concentrated at the subsurface layer for more than 30 d. Following this, the Chl *a* core (Fig. 7a) gradually moved towards the surface. Furthermore, we also noted the horizontal movement of the Chl *a* core. Comparing the evolution of Chl *a* distribution (Fig. 7a) with surface wind as shown in Fig. 8, we could determine the relationships between them. Over the entire period, the surface wind force played an important role in the distribution of *P. donghaiense*. Easterly winds prevailed from the 40th to 80th day, persistently pushing water along with *P. donghaiense* shoreward. During the last 10 d, the algal bloom was pushed off-shore by strong westerly winds.

Table 3. A preliminary hypothesis on motion during large-scale dinoflagellate blooms in the East China Sea (after Zhou and Zhu, 2006)

Bloom evolution	Motion
Initiating	Bottom→Subsurface Offshore→Nearshore
Developing	Subsurface
Proliferating	Surface
Dispersing	Surface→Subsurface→Bottom Nearshore→Offshore

The effects of surface wind fields on the horizontal and vertical distribution of algal blooms have been discussed in numerous previous investigations (Vanhoutte-Brunier et al., 2008; Li et al., 2009; Luo et al., 2012; McGillicuddy Jr et al., 2014; Son et al., 2015). In Fig. 9, we illustrated the distribution of Chl *a* over the last 6 d to highlight the dispersing stage since this stage was shorter than 10 d. At the end of the proliferating stage, the Chl *a* concentrated at the surface layers, where the higher synthesis rate resided. During the last 6 d, surface winds pushed the bloom off shore where the surface synthesis rate was limited by PO_4^{3-}. As a result, the bloom dispersed, with the Chl *a* core moving downward gradually and bypassing the P-limited area. This highlights the importance of surface wind forcing in the determination of the spatial distribution of blooms. This is consistent with the cell motion in the dispersing stage proposed by Zhou and Zhu (2006).

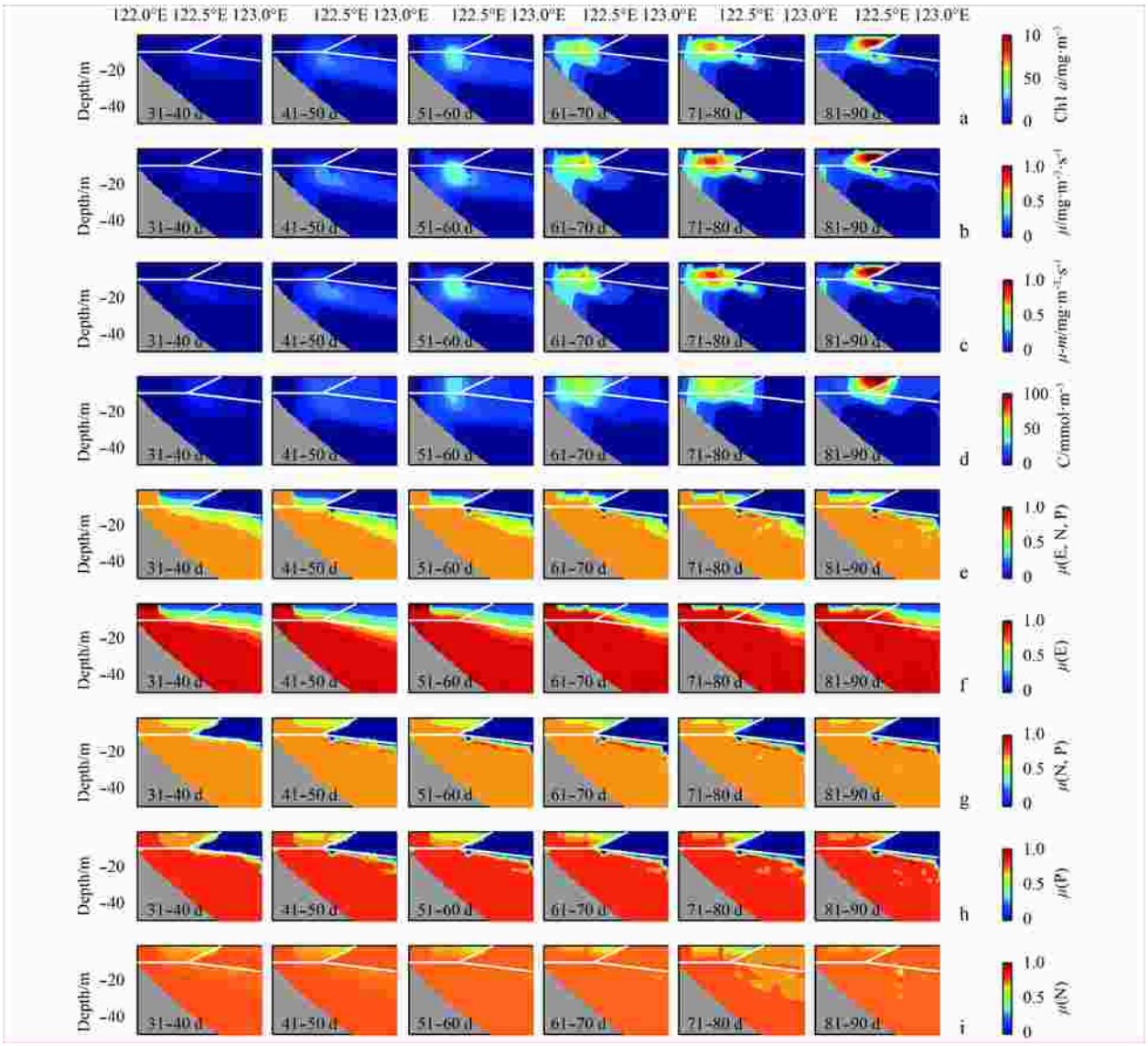

Fig. 7. Ten day-mean vertical distributions of modeled Chl *a* and terms regulating Chl *a* synthesis rates, ranging from 0 (total limitation) to 1 (no limitation). The section is located at the middle of the five sections shown in Fig. 6. μ(E) is light-limited term, and μ(N, P) is the nutrient-limited term determined by minimum (μ(N), μ(P)), according to the principle of Liebig's Law. μ(E, N, P) is determined by μ(E)×μ(N, P). The gross synthesis term (μ) is determined by μ(E, N, P) and C. The net synthesis term is μ-mortality (μ–m). The upper layer is divided into two parts by the white lines.

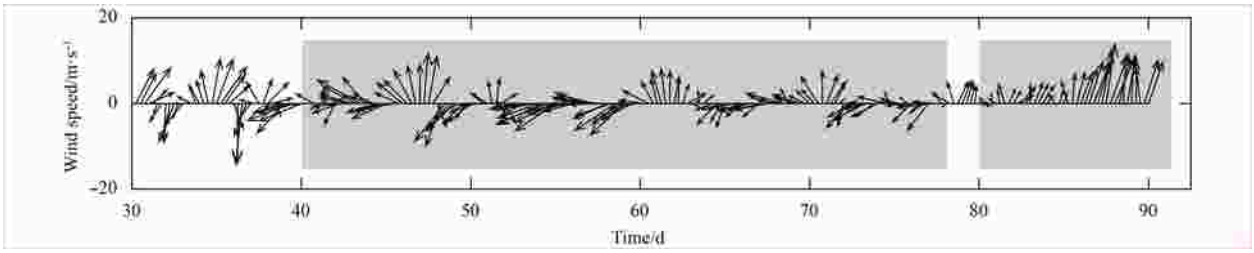

Fig. 8. Time series of wind vectors. Grey represents the easterly and westerly wind.

4.4 *Incubation at the subsurface layer*

Phytoplankton aggregation via *in-situ* growth can occur when growth is most vigorous at mid-depth, i.e., when growth is either light- or nutrient-limited, except over a small depth interval or when nutrients are abundant only at mid-depth (Durham and Stocker, 2012). As reported by Zhou and Zhu (2006), the subsurface incubation of *P. donghaiense* may be closely related to physical processes. They found that the subsurface temperature was more capable of supporting *P. donghaiense* growth due to the invasion of warm water, while the surface temperature was too low

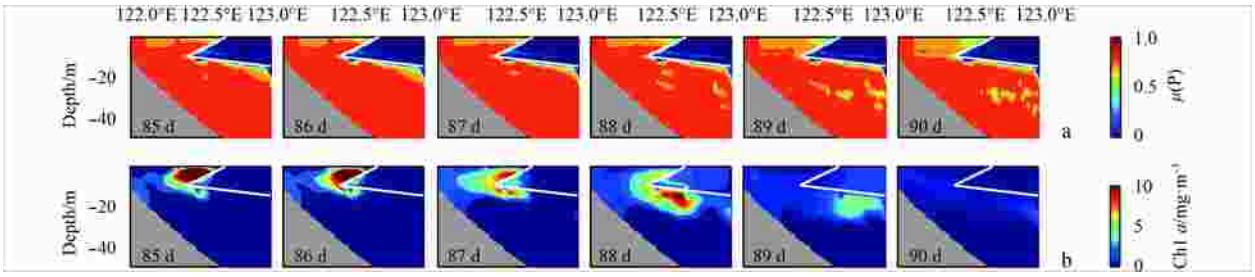

Fig. 9. The vertical distributions of modeled μ(P) (a) and Chl *a* (b) during the last 6 d. The section is located at the middle of the five sections shown in Fig. 6. The P-limited area is marked by the white outline.

in early April. Chen et al. (2006) indicated that the turbidity of coastal waters and the distribution of nutrients might lead to subsurface incubation. Until now, no definite conclusion has been established, with several factors suspected as the potential cause of subsurface incubation. Our simulated results emphasize the importance of nutrient limitation in this phenomenon; however, further investigations are needed to confirm the reliability of the present findings. In addition, several other mechanisms (including shear, convergent swimming, buoyancy, gyrotactic trapping, intrusions, and grazing) have been proposed. Two of these (convergent swimming and gyrotactic trapping) are related to dinoflagellate swimming. This vertical migration of dinoflagellates has been previously formulated in several models (He et al., 2008; Li et al., 2009) to investigate the development of algal blooms. In the present model, the vertical migration of *P. donghaiense* was not considered. Further addition of the swimming behavior and other formation mechanisms is a topic of ongoing research.

5 Conclusions

We designed a species-specific model for *P. donghaiense* that considered biological processes such as growth, uptake, and Chl *a* synthesis. By calibrating the parameters against experimental results, the biological model successfully reproduced the growth of *P. donghaiense* under various light and PO_4^{3-} availability scenarios. The biological model was integrated with the ROMS tailored for the ECS to analyze the spatiotemporal evolution of a *P. donghaiense* bloom in 2005. The coupled model faithfully reproduced the ECS coastal hydrodynamics and the observed *P. donghaiense* bloom off Zhejiang Province. Factors affecting the vertical evolution of the bloom along one typical section were analyzed through diagnosing various terms that regulated the Chl *a* synthesis rate.

The results revealed a significant influence of PO_4^{3-} on the vertical distributions of Chl *a* concentration. Furthermore, a forcing mechanism is proposed to explain the observed incubation in the subsurface waters, in addition to the dispersion of the bloom from the surface to the bottom. Surface wind fields played an important role in modulating the transportation, in the form of persistent easterly winds causing strong onshore transportation at the developing stage and strong westerly winds causing subsequent offshore transportation. The westerly winds also helped disperse the bloom, pushing the algal population off shore more quickly, where the Chl *a* synthesis was limited by PO_4^{3-}.

Collectively, our results are consistent with the observations proposed by earlier studies. Although the findings highlight the importance of nutrient-limitation in the formation of *P. donghaiense* subsurface layers and dispersing of *P. donghaiense* blooms, other biological factors, as well as hydrodynamic transport, may play important roles in determining the spatiotemporal structures of the bloom. Since *P. donghaiense* blooms are a recurrent problem in the ECS, the coupled model should be further improved and used under different scenarios.

Acknowledgements

The authors appreciate Zheng Quan'an for reviewing this paper and thank Melica Baklouti for sharing the Eco3M code. We are grateful to all reviewers for their constructive suggestions.

References

Baklouti M, Faure V, Pawlowski L, et al. 2006. Investigation and sensitivity analysis of a mechanistic phytoplankton model implemented in a new modular numerical tool (Eco3M) dedicated to biogeochemical modelling. Progress in Oceanography, 71(1): 34–58

Cannell M G R, Thornley J H M. 2000. Modelling the components of plant respiration: some guiding principles. Annals of Botany, 85(1): 45–54

Chen Hanlin, Lv Songhui, Zhang Chuansong, et al. 2006. A survey on the red tide of *Prorocentrum donghaiense* in East China Sea 2004. Ecologic Science (in Chinese), 25(3): 226–230

Chen Yang, Yan Tian, Zhou Mingjiang. 2007. Effects of *Prorocentrum donghaiense* and *Alexandrium catenella* on the material transfer in a simulated marine food chain. Shengtai Xuebao (in Chinese), 27(10): 3964–3972

Cullen J J. 1982. The deep chlorophyll maximum: comparing vertical profiles of chlorophyll *a*. Canadian Journal of Fisheries and Aquatic Sciences, 39(5): 791–803

Dai Fangfang, Zhou Chengxu, Yan Xiaojun. 2011. Effect of pH and light on population growth and activity of extracellular carbonic anhydrase in two species of dinoflagellates. Marine Environmental Science (in Chinese), 30(5): 694–698

Deng Ningning. 2004. Effect of dissolved inorganic nutrients composition on the growth of HAB algae in East China Sea (in Chinese) [dissertation]. Qingdao: Ocean University of China

Deng Guang, Geng Yahong, Hu Hongjun, et al. 2009. Effects of environmental factors on photosynthesis of a high biomass bloom forming species *Prorocentrum donghaiense*. Marine Sciences (in Chinese), 33(12): 34–39

Doherty J. 2004. PEST: Model Independent Parameter Estimation, User Manual. 5th ed. Brisbane, Australia: Watermark Numerical Computing

Droop M R. 1968. Vitamin B12 and marine ecology: IV. The kinetics of uptake, growth and inhibition in *Monochrysis lutheri*. Journal of the Marine Biological Association of the United Kingdom, 48(3): 689–733

Durham W M, Kessler J O, Stocker R. 2009. Disruption of vertical motility by shear triggers formation of thin phytoplankton layers. Science, 323(5917): 1067–1070

Durham W M, Stocker R. 2012. Thin phytoplankton layers: characteristics, mechanisms, and consequences. Annual Review of Marine Science, 4(4): 177–207

Guillard R R L. 1973. Division rates. In: Stein J R, ed. Handbook of Phycological Methods: Culture Methods & Growth Measure-

ments. Cambridge: Cambridge University Press, 289–311
He Ruoying, McGillicuddy Jr D J, Keafer B A, et al. 2008. Historic 2005 toxic bloom of *Alexandrium fundyense* in the western Gulf of Maine: 2. Coupled biophysical numerical modeling. Journal of Geophysical Research, 113(C7): C07040
Huang Bangqin, Ou Linjian, Hong Huasheng, et al. 2005. Bioavailability of dissolved organic phosphorus compounds to typical harmful dinoflagellate *Prorocentrum donghaiense* Lu. Marine Pollution Bulletin, 51(8–12): 838–844
Lai Junxiang, Yu Zhiming, Song Xiuxian, et al. 2011. Responses of the growth and biochemical composition of *Prorocentrum donghaiense* to different nitrogen and phosphorus concentrations. Journal of Experimental Marine Biology and Ecology, 405(1–2): 6–17
Li Ying. 2006. The Eco-physiological studies of phosphorus on the growth of *Prorocentrum donghaiense* (in Chinese) [dissertation]. Guangzhou: Jinan University
Li Yizhen, He Ruoying, McGillicuddy Jr D J, et al. 2009. Investigation of the 2006 *Alexandrium fundyense* bloom in the Gulf of Maine: In-situ observations and numerical modeling. Continental Shelf Research, 29(17): 2069–2082
Li Yang, Lü Songhui, Jiang Tianjiu, et al. 2011. Environmental factors and seasonal dynamics of *Prorocentrum* populations in Nanji Islands National Nature Reserve, East China Sea. Harmful Algae, 10(5): 426–432
Lu Rong. 2005. Dynamic study and influence of nutrients to the growth of phytoplankton in mesocosm experiments of East China Sea (in Chinese) [dissertation]. Qingdao: Ocean University of China
Luo Lin, Wang Jia, Schwab D J, et al. 2012. Simulating the 1998 spring bloom in Lake Michigan using a coupled physical-biological model. Journal of Geophysical Research, 117(C10): C10011
McGillicuddy Jr D J, Brosnahan M L, Couture D A, et al. 2014. A red tide of *Alexandrium fundyense* in the Gulf of Maine. Deep Sea Research Part II: Topical Studies in Oceanography, 103(3): 174–184
McManus M A, Kudela R M, Silver M V, et al. 2008. Cryptic blooms: are thin layers the missing connection. Estuaries and Coasts, 31(2): 396–401
Ou Linjian, Wang Dan, Huang Bangqin, et al. 2008. Comparative study of phosphorus strategies of three typical harmful algae in Chinese coastal waters. Journal of Plankton Research, 30(9): 1007–1017
Rines J E B, Donaghay P L, Dekshenieks M M, et al. 2002. Thin layers and camouflage: hidden *pseudo-nitzschia* spp. (Bacillariophyceae) populations in a fjord in the San Juan Islands, Washington, USA. Marine Ecology Progress Series, 225(1): 123–137
Rines J E B, McFarland M N, Donaghay P L, et al. 2010. Thin layers and species-specific characterization of the phytoplankton community in Monterey Bay, California, USA. Continental Shelf Research, 30(1): 66–80
Shchepetkin A F, McWilliams J C. 2005. The regional oceanic modeling system (ROMS): a split-explicit, free-surface, topography-following-coordinate oceanic model. Ocean Modelling, 9(4): 347–404
Son Y B, Choi B J, Kim Y H, et al. 2015. Tracing floating green algae blooms in the Yellow Sea and the East China Sea using GOCI satellite data and Lagrangian transport simulations. Remote Sensing of Environment, 156(156): 21–33
Song Yuhe, Haidvogel D. 1994. A semi-implicit ocean circulation model using a generalized topography-following coordinate system. Journal of Computational Physics, 115(1): 228–244
Sullivan J M, Donaghay P L, Rines J E B. 2010. Coastal thin layer dynamics: consequences to biology and optics. Continental Shelf Research, 30(1): 50–65
Sullivan J M, Swift E, Donaghay P L, et al. 2003. Small-scale turbulence affects the division rate and morphology of two red-tide dinoflagellates. Harmful Algae, 2(3): 183–199
Sullivan J M, Twardowski M S, Donaghay P L, et al. 2005. Use of optical scattering to discriminate particle types in coastal waters. Applied Optics, 44(9): 1667–1680
Sun Shugang. 2010. Uptake and utilization characteristics of *Prorocentrum donghaiense* for urea (in Chinese) [dissertation]. Guangzhou: Jinan University
Sun Suihan, Duan Shunshan. 2006. Effect of photoperiod on marine microalgae *Prorocentrum donghaiense*. Ecology and Environment (in Chinese), 15(3): 461–464
Sun Ke, Qiu Zhongfeng, He Yijun, et al. 2014. Nutrient-controlled growth of Skeletonema costatum: an applied model. Chinese Journal of Oceanology and Limnology, 32(3): 608–625
Sun Ke, Qiu Zhongfeng, He Yijun, et al. 2016. Succession of causative species during spring blooms in the East China Sea: coupled biophysical numerical modeling. Acta Oceanologica Sinica, 35(12): 1–11
Sun Baiye, Wang Xiulin, Li Yanbin, et al. 2008. Effects of irradiance on blooms of the dinoflagellate *Prorocentrum donghaiense* Lu in the coastal area in East China Sea. Environmental Science (in Chinese), 29(2): 362–367
Tang Jingliang, Mao Hongyue, Guo Meirong. 2006. Analysis on the red tide of *Prorocentrum dantatum* in the north coastal water of Zhejiang. Marine Environmental Science (in Chinese), 25(3): 63–66
Vanhoutte-Brunier A, Fernand L, Ménesguen A, et al. 2008. Modelling the *Karenia mikimotoi* bloom that occurred in the western English Channel during summer 2003. Ecological Modelling, 210(4): 351–376
Xu Ning. 2006. A study on niche of representative harmful algal bloom species in the coastal waters of China (in Chinese) [dissertation]. Guangzhou: Jinan University
Xu Ning, Duan Shunshan, Li Aifen, et al. 2010. Effects of temperature, salinity and irradiance on the growth of the harmful dinoflagellate *Prorocentrum donghaiense* Lu. Harmful Algae, 9(1): 13–17
You Xihua. 2006. Studies on the growth of *Prorocentrum donghaiense* and *Alexandrium tamarense* under different environmental factor and the interspecific competition (in Chinese) [dissertation]. Qingdao: Ocean University of China
Zhang Chuansong. 2008. The characteristic and effects of nutrient during the process of HAB in Changjiang River estuary and its adjacent area (in Chinese) [dissertation]. Qingdao: Ocean University of China
Zhang Chuansong, Wang Jiangtao, Zhu Dedi, et al. 2008. The preliminary analysis of nutrients in harmful algal blooms in the East China Sea in the spring and summer of 2005. Haiyang Xuebao (in Chinese), 30(2): 153–159
Zhao Shuidong. 2006. Study on the effect of temperature, salinities and nutritions on the growth of *Prorocentrum dentatum* (in Chinese) [dissertation]. Guangzhou: Jinan University
Zhao Yanfang, Yu Zhiming, Song Xiuxian, et al. 2009. Comparative research on the effects of different nutrient concentrations on the photopigment content and photosynthesis of two bloom-forming species isolated from the Changjiang River Estuary. Environmental Science (in Chinese), 30(3): 700–706
Zhou Mingjiang, Yan Tian, Zou Jingzhong. 2003. Preliminary analysis of the characteristics of red tide areas in Changjiang River estuary and its adjacent sea. Chinese Journal of Applied Ecology (in Chinese), 14(7): 1031–1038
Zhou Weihua, Yin Kedong, Zhu Dedi. 2006. Phytoplankton biomass and high frequency of Prorocentrum donghaiense harmful algal bloom in Zhoushan sea area in spring. Chinese Journal of Applied Ecology (in Chinese), 17(5): 887–893
Zhou Mingjiang, Zhu Mingyuan. 2006. Progress of the project "ecology and oceanography of harmful algal blooms in China". Advances in Earth Science (in Chinese), 21(7): 673–679
Zhu Dedi, Lu Douding, Wang Yunfeng, et al. 2009. The low temperature characteristics in Zhejiang coastal region in the early spring of 2005 and its influence on harmful algae bloom occurrence of *Prorocentrum donghaiense*. Haiyang Xuebao (in Chinese), 31(6): 31–39

Appendix:

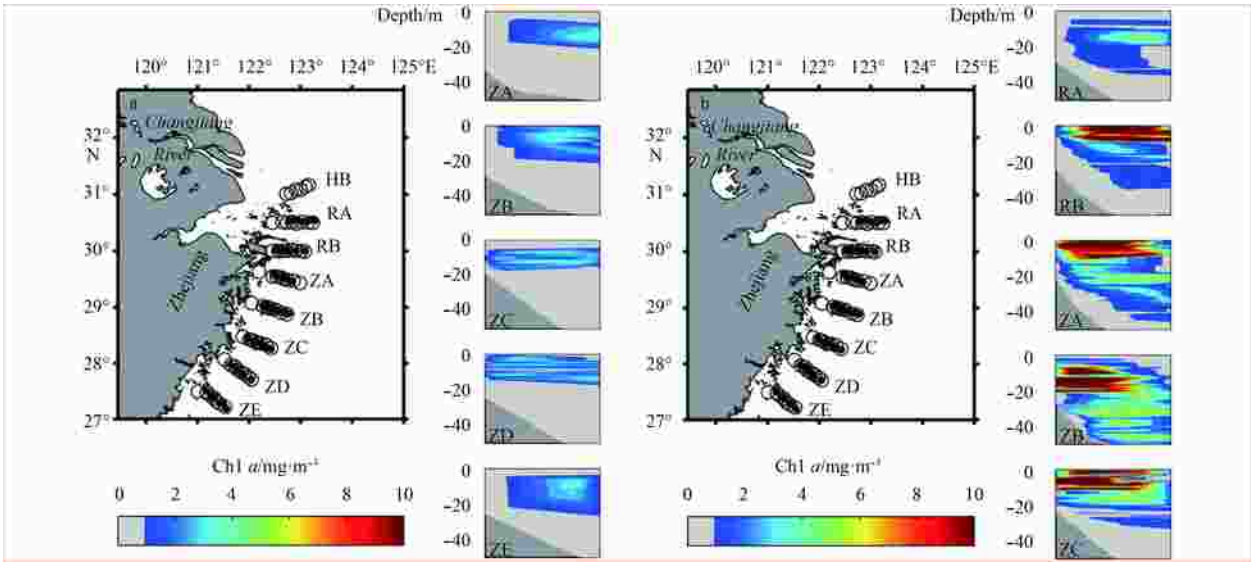

Fig. A1. Survey stations during the 2004 cruises (solid circle) and the development of the *P. donghaiense* bloom between April (a) and May (b) at the subsurface layer (after Zhou and Zhu, 2006). Survey stations during the 2005 cruise (blank square) are also presented to show the similarity of sections between the two years. Eight coast-scale ship surveys were executed between March 27 and June 24 in 2005, covering the entire coastal region. Nutrient data acquired from the survey were utilized in the model and a detailed description of the sampling method can be found in Zhang et al. (2008).